Hindawi Publishing Corporation
Shock and Vibration
Volume 2014, Article ID 489090, 11 pages
http://dx.doi.org/10.1155/2014/489090

Review Article

A Numerical Study of the Screening Effectiveness of Open Trenches for High-Speed Train-Induced Vibration

Chih-hung Chiang and Pei-hsun Tsai

Department of Construction Engineering, Chaoyang University of Technology, 168 Jifong E. Road, Wufeng District, Taichung 41349, Taiwan

Correspondence should be addressed to Pei-hsun Tsai; phtsai@cyut.edu.tw

Received 29 March 2013; Revised 5 November 2013; Accepted 23 January 2014; Published 27 February 2014

Academic Editor: Nuno Maia

This study used the 2D boundary element method in time domain to examine the screening effectiveness of open trenches on reducing vibration generated by a high-speed train. The parameters included configurations of the trench, train speed, the distance between the source and the trench, and the Poisson's ratio of the soil. A reducing displacement level (in dB scale) was defined and used to evaluate the screening effectiveness of a wave barrier. The maximal reducing displacement level reached 25 dB when an open trench was used as a wave barrier. The depth of an open trench is a main influential parameter of screening effectiveness. The cutoff frequency of the displacement spectrum increases with decreasing trench depth. The maximal screening effectiveness occurs when the depth is 0.3-0.4 Rayleigh wavelength. Using an open trench as a wave barrier can reduce 10–25 dB of vibration amplitude at frequencies between 30 and 70 Hz. A considerable increase in screening effectiveness of the open trench was observed from 30 to 70 Hz, which matches the main frequencies of vibration induced by Taiwan High Speed Rail. The influence of trench width on screening effectiveness is nonsignificant except for frequencies from 30 to 40 Hz. Poisson's ratio has various effects on the reduction of vibration at frequencies higher than 30 Hz.

1. Introduction

High-speed trains (HSTs) have played an essential role in intercity transportation during the past decades. The weight of freight trains and the speed of passenger trains have increased. Trains passing populated areas result in ground vibration and cause disturbances to adjacent structures. Reducing vibration in nearby structures has become a crucial issue in practice. Installation of barriers (such as a row of concrete piles or steel pipe piles and open trench or infilled trench) between tracks and the structures is one solution of isolation vibration. An open trench is often used as a wave barrier causing reflection, scattering, and diffraction effects. The vibration amplitude is thus reduced on the ground surface behind the open trench. Elastomer or rubber between the ballast and subgrade, soil improvement underneath the track, and floating slab track are other effective methods to reduce vibration induced by train.

A number of experimental and numerical studies [1–4] have been conducted to examine the ground vibration induced by HSTs. These studies mainly focused on the ground vibration generated by HSTs. In addition, the screening effectiveness of trenches on harmonic vibration sources generated by machine foundations has also been investigated in the last few decades [5–9]. Because of single frequency vibration on foundations, it is suitable to analyze the vibration response on a ground surface using the frequency domain boundary element method (BEM). These studies indicated considerable wave isolation effectiveness for open trenches with sufficient depth. The vibration-induced HSTs can be of multiple frequencies or expressed as a function of frequency. However, the screening effectiveness of open trenches on vibrations requires analyses different from those based on harmonic vibration because HSTs induced vibrations of many frequencies. Only a few studies have focused on barriers to reduce vibration caused by HSTs. Takemiya [10] used finite element method (FEM) to study vibration mitigation of

honeycomb wave impending barrier induced by the Taiwan high-speed train on a viaduct construction. Hung et al. [11] used a 2.5D finite/infinite element method to study the reduction of vibration of wave barriers induced by various train speeds. The parameters that influence the reduction of amplitude under investigation include the type of wave barrier and the speed of trains. Andersen and Nielsen [12] used the coupled finite element-boundary element model to perform a parametric study on the influence of trench barrier and soil improvement underneath the track on the level of ground vibration. Karlström and Boström [13] used an analytical approach with Fourier transform and Fourier series to examine the influence of open trenches on vibration reduction. Cao et al. [14] used an analytical model to analyze the screening effectiveness of open trenches for reducing vibration induced by a moving rectangular load on a fully saturated poroelastic half-space. Younesian and Sadri [15] used FEM to investigate the effect of the trench geometry on isolation vibration induced by HSTs. Celebi and Kırtel [16] investigated the effects of the nonlinear behavior of soil on screening performance of thin-walled trench barriers for reducing train-induced ground vibrations by using a finite element code.

Many researchers applied frequency-domain BEM and sometimes in conjunction with FEM to the investigations on the effectiveness of reducing the vibration induced by HSTs. However, the vibration-induced HSTs is a transient wave propagation analysis; a time-domain BEM is more appropriate. Adam and von Estorff [18] used time-domain coupled boundary element-finite element method to study the effectiveness of open trench and infilled trenches on reducing the building vibrations induced by train. The applied load time history is assumed as 4-rectangle impulses. The isolation effectiveness of trench was evaluated by the difference of the maximum values in time domain between with/without trench barriers.

The relationship between the dominant frequencies of HSTs and the frequency range of reducing ground vibration using an open trench has not been fully examined. To study the main frequency range of isolation vibration for different open trenches, parametric studies were performed by varying the dimensions and locations of an open trench, including width, depth of the trench, the source distance from the trench to the center of the vibration source, soil Poisson's ratio, and the speed of trains. The time-domain BEM was used to analyze the vibration isolation problem in this study since it requires only surface discretization and automatically satisfies the radiation conditions at infinite boundary.

2. Numerical Method

Although soil is an elastic-plastic material, we can assume the properties of an elastic material because the strain induced by HSTs is small. The governing equation of dynamic equilibrium for an elastic, isotropic, and homogeneous medium is a Navier-Cauchy equation:

$$\mu\nabla^2 u_i(x,t) + (\lambda+\mu)\nabla\nabla\cdot u_i(x,t) + \rho b_i(x,t) = \rho\frac{\partial^2 u_i(x,t)}{\partial t^2}, \tag{1}$$

where u is the displacement vector; x is the position vector; t is the time; b is the body force vector; and ρ is the mass density. λ and μ are the Lamé constants, and the subscripts $i, j = 1, 2$. If the contribution of the body force is neglected and the initial displacement and velocity of the medium are zero, the boundary integral equation, obtained using Graffi's dynamic reciprocal theorem between the actual state and the fundamental solution state, can be expressed as follows:

$$\begin{aligned} c_{ij}(\xi)\, u_i(\xi,t) &= \int_s \left[\int_0^t G_{ij}(x,t-\tau,\xi)\, t_i(x,\tau)\, d\tau \right. \\ &\quad \left. - \int_0^t F_{ij}(x,t-\tau,\xi)\, u_i(x,\tau)\, d\tau\right] ds(x), \end{aligned} \tag{2}$$

where $u_i(x,\tau)$ and $t_i(x,\tau)$ are the displacement and traction of barrier reducing vibration system, respectively. x and ξ are the field and source points, respectively. $G_{ij}(x,\tau,\xi)$ and $F_{ij}(x,\tau,\xi)$ are the 2D displacement and traction fundamental solutions, respectively. c_{ij} is a well-known discontinuity term resulting from the singularity of the F_{ij}-kernel and is treated using the sense of Cauchy principal value.

The corresponding elastodynamic displacement fundamental equation for 2D [19] is as follows:

$$G_{ij}(x,t,\xi) = \frac{1}{2\pi\rho}\left\{\frac{1}{c_1}g_1 - \frac{1}{c_2}g_2\right\}, \tag{3}$$

where c_1 is the velocity of the dilatational wave and c_2 is the velocity of the shear wave, and

$$\begin{aligned} g_1 &= \begin{cases} \dfrac{2(c_1 t/r)^2 - 1}{\left[(c_1 t/r)^2 - 1\right]^{0.5}}\left(\dfrac{r_{,i}r_{,j}}{r}\right) - \dfrac{\delta_{ij}}{r}\sqrt{\left(\dfrac{c_1 t}{r}\right)^2 - 1} & \text{if } \dfrac{c_1 t}{r} > 1, \\ 0 & \text{if } \dfrac{c_1 t}{r} < 1, \end{cases} \\ g_2 &= \begin{cases} \dfrac{2(c_2 t/r)^2 - 1}{\left[(c_2 t/r)^2 - 1\right]^{0.5}}\left(\dfrac{r_{,i}r_{,j}}{r}\right) - \dfrac{\delta_{ij}}{r}\dfrac{(c_2 t/r)^2}{\sqrt{(c_2 t/r)^2 - 1}} & \text{if } \dfrac{c_2 t}{r} > 1, \\ 0 & \text{if } \dfrac{c_2 t}{r} < 1, \end{cases} \end{aligned} \tag{4}$$

where r denotes the vector from the source point ξ to field point x, δ_{ij} is the Kronecker delta, and the inferior commas indicate space derivatives.

The 2D elastodynamic traction fundamental solution [19] is expressed as follows:

$$F_{ij}(x,t,\xi) = \frac{\mu}{2\pi\rho r}\left\{\frac{1}{c_1}H\left(\frac{c_1 t}{r}-1\right)\left[\frac{1}{\left((c_1 t/r)^2-1\right)^{1.5}}\left(\frac{A_{ij}^1}{r}\right) + \frac{2(c_1 t/r)^2-1}{\left((c_1 t/r)^2-1\right)^{0.5}}\left(\frac{2A_{ij}^2}{r}\right)\right] - \frac{1}{c_2}H\left(\frac{c_2 t}{r}-1\right)\left[\frac{1}{\left((c_2 t/r)^2-1\right)^{1.5}}\left(\frac{A_{ij}^3}{r}\right) + \frac{2(c_2 t/r)^2-1}{\left((c_2 t/r)^2-1\right)^{0.5}} \times\left(\frac{2A_{ij}^2}{r}\right)\right]\right\}, \tag{5}$$

where H is the Heaviside function, and

$$A_{ij}^1 = \left(\frac{\lambda}{\mu}\right)n_j r_{,i} + 2r_{,i}r_{,j}\frac{\partial r}{\partial n},$$
$$A_{ij}^2 = n_i r_{,j} + n_j r_{,i} + \frac{\partial r}{\partial n}\left(\delta_{ij} - 4r_{,i}r_{,j}\right), \tag{6}$$
$$A_{ij}^3 = \frac{\partial r}{\partial n}\left(2r_{,i}r_{,j} - \delta_{ij}\right) - n_i r_{,j},$$

where n is the unit outward normal vector at field point x. The boundary S of the medium in (2) is divided into M boundary elements, and the time axis is divided into N equal steps. After completing the temporal and spatial integration, (2) can be simplified to a system of algebraic equations. It can be expressed as a matrix form:

$$\sum_{n=1}^{N}\left(\left[G^{N-n+1}\right]\{t^n\} - \left[F^{N-n+1}\right]\{u^n\}\right) = \{0\}, \tag{7}$$

where $\{t^n\}$ and $\{u^n\}$ are vectors of the nodal tractions and displacements, respectively, with the superscript referring to the time-step index.

At step N, only half of the boundary variables are unknown. All boundary variables at steps less than N are obtained. By substituting the boundary condition into (7), the following governing equation can be obtained:

$$\left[A^1\right]\left\{X^N\right\} = \left[B^1\right]\left\{Y^N\right\} - \sum_{n=1}^{N-1}\left(\left[G^{N-n+1}\right]\{t^n\} - \left[F^{N-n+1}\right]\{u^n\}\right). \tag{8}$$

The unknown vector $\{X^N\}$ at step N in (8) can be solved using the Gaussian elimination method. Subsequently, the displacement and traction of all boundary elements can be obtained.

Israil and Banerjee [17] proposed simplified formulation on time-domain BEM; the parametric studies of open trench was not performed and the applied load time history was a triangular impulsive which is not similar to the trainloads of high speed train. This study adopted the simplified formulation [17] and 2D elastodynamic fundamental solution to code a FORTRAN program. To verify the BEM code developed in this study, a numerical analysis on the vibration before and after the trench was compared with the results from Israil and Banerjee [17], as shown in Figure 1. The boundary elements mesh and the applied loads which were used by Israil and Banerjee [17] are shown in Figure 1(a). The assumed material properties of soil are as follows: shear modulus $G = 132\,\mathrm{MN/m^2}$, Poisson's ratio $\nu = 0.25$, density $\rho = 1785.7\,\mathrm{kg/m^3}$, and shear wave velocity $c_2 = 271.88\,\mathrm{m/s}$. The material damping was not included in this study. The time increment was 0.002 s, and the length of all elements was 0.5 m. A uniform traction was subjected to a zone of $2b = 2\,\mathrm{m}$ in width. The time history of traction was a triangular impulse (amplitude of impulse $P = 1\,\mathrm{MN/m^2}$) the rise-time of the load was 0.002 s, and the duration of the load was 0.004 s. The open trench (width: $W = 1\,\mathrm{m}$ and depth: $H = 3\,\mathrm{m}$) was located at a distance of 10 m from the edge of the loading zone. The vertical displacement time history, $u_y(t)$, at both points on the ground surface were recorded; Point A (10 m from center of the loading zone) and Point B (13 m from center of the loading zone) are before and after the open trench, respectively. Using a graphical comparison, the results in Figure 1 are similar to those obtained by Israil and Banerjee [17], especially for Point B (after open trench). This validated the accuracy of the developed BEM code for screening the effectiveness of an open trench.

3. Numerical Model

The numerical program used in this study was coded according to time-domain boundary element theory using FORTRAN language. A typical mesh for the spatial domain was discretized using 106 boundary elements, as shown in Figure 2. The duration of the vibration was 2 s and time increment was 0.002 s. The total number of steps was 1000. The finest element size was used (approximately 0.25 m) on the surface of the trench and the ground surface areas near the trench. The boundary element sizes were set to 0.5 m on the ground surface behind the trench.

As shown in Figure 2, an open trench (depth H, width W) is located at a distance L from the center of two traces subjected to a load history of 4 HST carriages. The weight of each carriage is approximately 500 kN and the length of each carriage is 25 m. The distance of traces was assumed to be 1.5 m. The wheel loading was considered as a triangular impulse load, and the magnitude was 62.5 kN. The wheel loading was expressed as a traction type because of the requirement of (3). The size of the load element was 0.25 m,

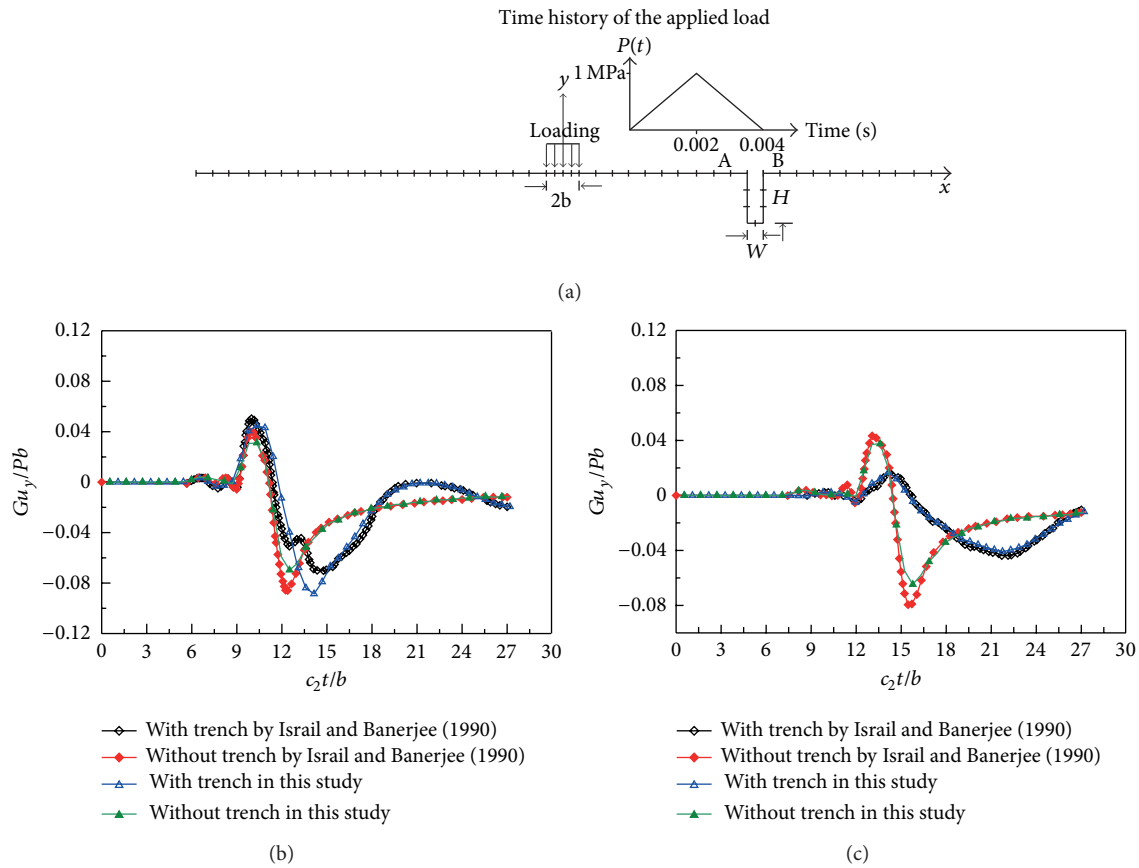

Figure 1: Effect of open trench on transient vibration: (a) boundary elements mesh and the applied loads were used by Israil and Banerjee [17], (b) displacement time history at Point A (before open trench), and (c) displacement time history at Point B (after open trench).

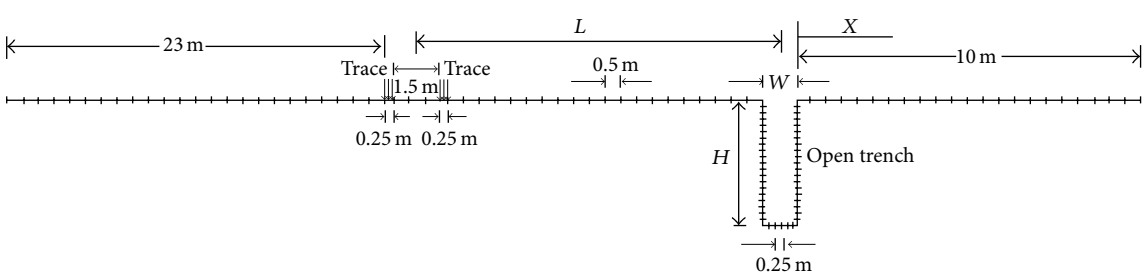

Figure 2: The typical mesh of open trench model.

and the amplitude of impulse traction was assumed as 250 kN/m^2. The loading history of 16 wheel loadings was added to the load elements, and the duration of each traction impulse was 0.004 s, as shown in Figure 3. Zero traction was assumed (traction free) for elements on the ground surface. The tractions were also assumed as zero for elements of the open trench.

The trainloads were modeled as 16 triangular impulse loads in this study. To verify the rationality of the assumption, a FEM was used to analyze the stress time history in wheel-rail-sleeper model. We assumed that the model includes three sleepers under the rail and wheel. The material properties of sleeper, rail, and wheel are listed in Table 1. The FEM mesh of wheel-rail-sleeper model is shown in Figure 4. When a wheel moves along the rail, von Mises stresses on the midpoint of center sleeper, and contact points of wheel-rail and rail-sleeper were recorded. The von Mises stress time history in the above positions was shown in Figure 5. In Figure 5, there are some large undulations of peaks in each stress time history figure. However, the macroscopic shape of stress time history on a rail is close to a triangle. This is why we have assumed a triangular impulse load in Figure 1(a). The shape of stress time history under a sleeper is irregular. From the above results, more high-frequency vibrations were generated because of more impulses in load time history. It can be because more high-frequency vibrations are generated when

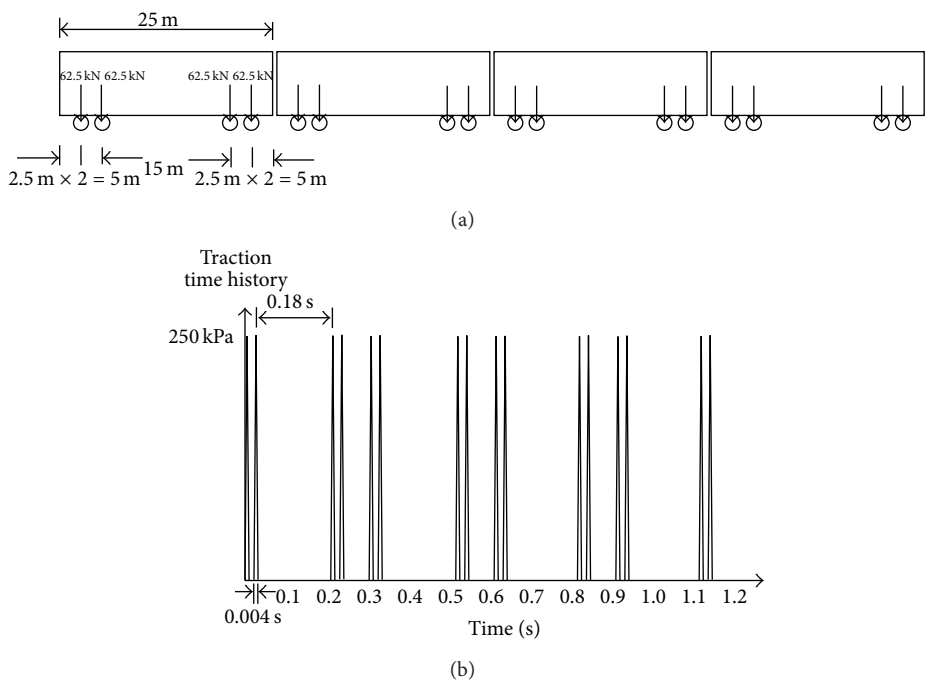

Figure 3: (a) The dimension of a high speed train (4 carriages) and (b) traction time history of wheel loading.

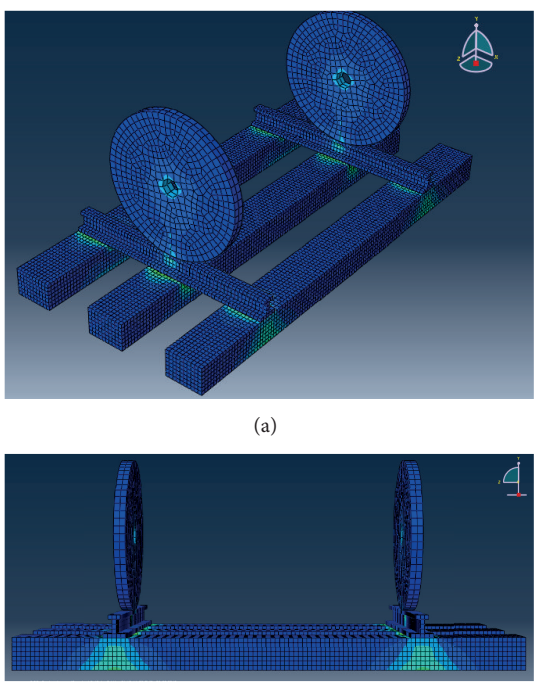

Figure 4: Finite element mesh of wheel-rail-sleeper model.

the wheel loading is applied on the elastic sleepers or rail. The authors considered a wheel load assumed as a triangular impulse applied on ground surface is helpful to perform numerical analysis due to load simplifying.

Table 1: Material properties of wheel, rail, and sleeper.

	Wheel and rail	Sleeper
Density (kg/m^3)	7800	160
Young's modulus (N/m^2)	2.05×10^{11}	5×10^9
Poisson's ratio	0.29	0.29

Fourier analysis cannot provide information on the frequency content of the changes in a signal over time. Time-frequency analysis can be performed with a CWT to understand the transient changes in the spectra. To transform an original signal into the form of dilation parameter and time, a wavelet function is used to perform the translation and dilation processes. The Morlet wavelet function was used to transform the time history of trainloads into the transformed value, which is indicated by dilation parameter and time. This study used the value of 0.5 Hz as the center frequency of the Morlet complex wavelet. The Morlet complex wavelet function $\psi(t)$ is defined as follows [20]:

$$\psi(t) = \pi^{-0.25}\left(e^{i2\pi f_c t} - e^{-(2\pi f_c)^2/2}\right)e^{-t^2/2}. \quad (9)$$

The transformed figure shows the distribution of the transform trainloads at the time-frequency plane, so that the characteristics of the trainloads in the time domain or frequency domain can be obtained simultaneously. Figure 6 shows the result of continuous wavelet transform to analyze the time-frequency characteristic of four-carriage loads. The amplitudes of transformed value are presented as a surface plot. In the figure, the near-zero values of continuous wavelet transform are distributed at larger values of the dilation parameter. Because frequencies are inversely proportional to

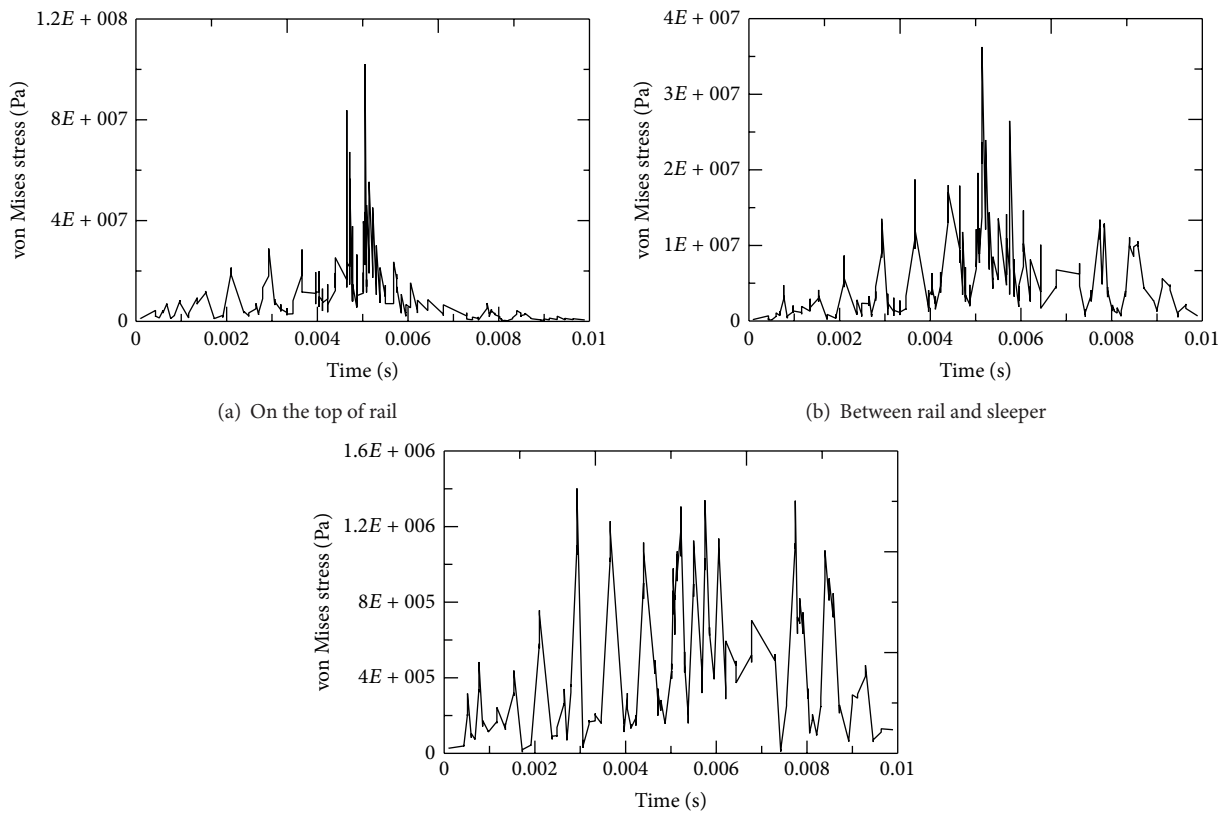

(a) On the top of rail

(b) Between rail and sleeper

(c) Under sleeper

Figure 5: Time history of contact stress figure.

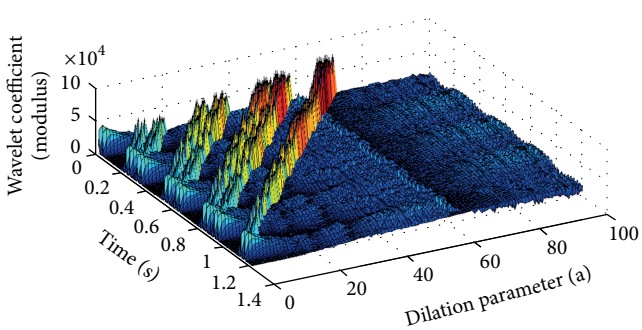

Figure 6: Time-frequency spectrum of the trainload of HSTs (4 carriages) using wavelet transform.

the dilations, the relationship between frequency and the dilation is defined as follows [20]:

$$f = \frac{f_c}{a\Delta_t}, \tag{10}$$

where f_c is the center frequency of a wavelet ($f_c = 0.5$ Hz), a is the dilation parameter, and Δ_t is the sample period. Large undulations of peaks exist at dilation values between 4 and 70 as shown in Figure 6. Sixteen peak values corresponded to the wheel loadings of a train. The frequency range of the train loading was from 3.6 to 62.5 Hz, calculated using (10). The assumption of soil properties includes Rayleigh wave velocity $c_R = 250$ m/s, density $\rho = 1785.7$ kg/m^3, and Poisson ratio $\nu = 0.25$. Stiff soil may ensure safe support of the HST. Therefore, the range of Rayleigh wavelength λ_R was estimated from 4 to 70 m. The typical mesh for the domain was discretized using 116 boundary elements when $L = 10$ m, $W = 1$ m, and $H = 3$ m, as shown in Figure 2. The finest element size of 0.25 m was used (approximately $\lambda_R/16$ in size as the frequency approached 62.5 Hz) on the surface of the open trench. The size of the element was 0.5 m (approximately $\lambda_R/8$ in size as the frequency approached 62.5 Hz) on the ground surface. Each element had two displacement directions. Therefore, the numerical model had 232 degrees of freedom. Because the velocity of the P wave was approximately 470 m/s and the time increment Δt was 0.002 s, the element size of the mesh was suitable. This study examined several configuration combinations of the open trench, speed of the train, and soil Poisson's ratio. The dimensions and other parameters are listed in Table 2.

4. Results of Numerical Analysis

4.1. Frequency Spectrum of Trainload. The normalized displacement spectrum for four-carriage trainloads with the speed of the train of 300 km/h was analyzed, as shown in Figure 7. The assumed material properties of soil were the

Table 2: Parameters for numerical analysis.

Purpose of analysis	Fixed parameters			Varying parameters
Influence of trench depth H	W	L	V	H
	1 m	10 m	300 km/h	2 m, 3 m, 5 m
Influence of trench width W	H	L	V	W
	3 m	10 m	300 km/h	1 m, 2 m, 4 m
Influence of source distance L	W	H	V	L
	1 m	3 m	300 km/h	10 m, 15 m, 17.5 m, 20 m
Influence of train speed V	W	H	L	V
	1 m	3 m	10 m	180 km/h, 225 km/h, 300 km/h

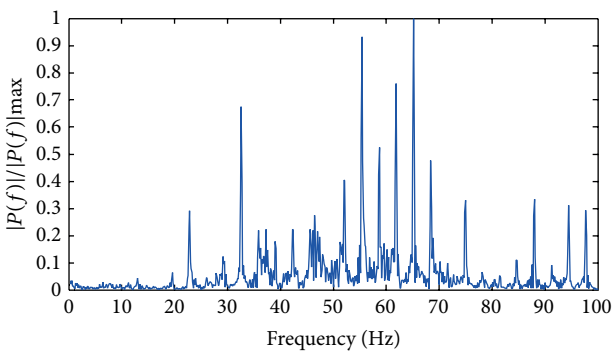

Figure 7: The displacement spectrum of experimental data (Taiwan High Speed Rail).

same of the aforementioned. The frequency spectrum of the trainload is similar to the theoretical result proposed by Ju et al. [4] when the speed of the train is 300 km/h and the distance between two carriage centers is 25 m. It implies that the assumed frequency spectrum of four-carriage trainloads is same as that of twelve-carriage trainloads [4].

For comparison, the ground vibration near the trace using the developed BEM code was compared with the measured result from the Taiwan High Speed Rail (THSR, 12 carriages). A comparison of the numerical and experimental results indicated a similar trend in the spectrum, except in a low frequency range. The amplitude on frequencies $f = 33$ and 67 Hz is larger than that other frequencies. Figure 7 shows the large amplitude of ground vibration induced by THSR. The dominant frequency of ground vibration near the track obtained from the experimental data is in the range from 30 to 70 Hz; a similar result was reported by Degrande and Schillemans [1].

4.2. Location-Frequency Spectrum Analysis of Ground Vibration. The location-frequency spectrum figures were provided so as to illustrate the isolation effectiveness before and after the open trench. The vibration time histories were transformed to a frequency spectrum using Fourier transform. The location-frequency spectrum figures are shown in Figures 8–11 and were used to examine the vibration isolation of a trench at various frequencies. Figure 8 shows a location-frequency spectrum figure in the case of a ground surface without a

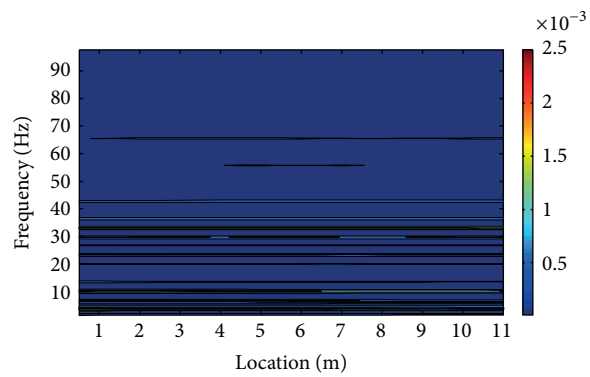

(a)

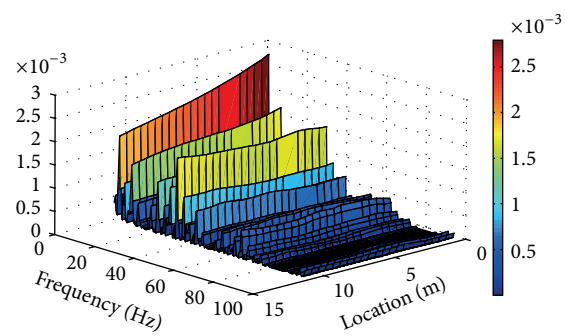

(b)

Figure 8: Location-frequency figure without wave barrier (a) contour plot of displacement spectrum on ground surface and (b) surface plot of displacement spectrum on ground surface (Poisson's ratio $\nu = 0.25$; train speed $V = 300$ km/h).

wave barrier and train speed of $V = 300$ km/h. Figures 9–11 show location-frequency spectrum figures in the case of an open trench with width of $W = 1$ m, depth of $H = 3$ m, and distance of $L = 10$ m between the vibration source and trench. The origin of the location coordinate was located at a distance of 2.5 m from the left edge of the trench; that is, the coordinate of the trench was from 2.5 m to 3.5 m. Figure 8 shows that the vibration of the train is concentrated on several frequencies. The amplitudes at frequencies larger than 80 Hz are less than those of other frequencies. The amplitude of ground vibration decreases with increasing distance from the vibration source only at frequencies lower than 20 Hz.

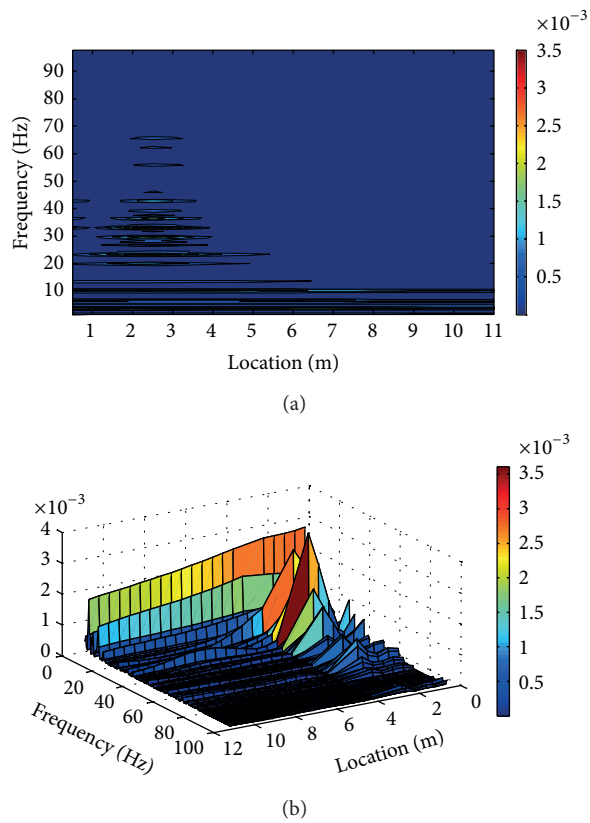

Figure 9: Location-frequency figure with an open trench of L = 10 m, W = 1 m, H = 3 m (a) contour plot of displacement spectrum on ground surface and (b) surface plot of displacement spectrum on ground surface (Poisson's ratio ν = 0.25; train speed V = 300 km/h). Note: the location coordinate of trench is from 2.5 to 3.5 m.

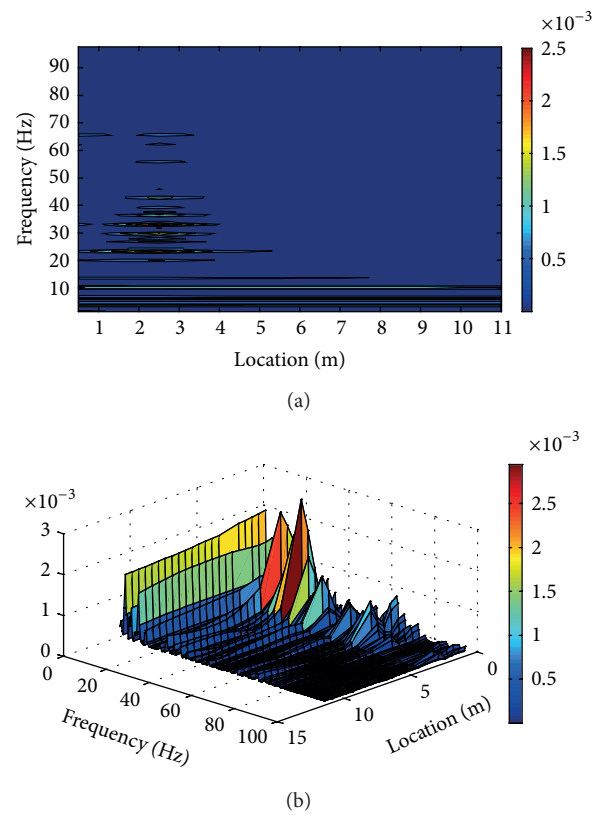

Figure 10: Location-frequency figure with an open trench of L = 10 m, W = 1 m, and H = 3 m (a) contour plot of displacement spectrum on ground surface and (b) surface plot of displacement spectrum on ground surface (Poisson's ratio ν = 0.45, train speed V = 300 km/h). Note: the location coordinate of trench is from 2.5 to 3.5 m.

Figure 9 shows the location-frequency spectrum figure for a trench with width of W = 1 m, depth of H = 3 m, and distance of L = 10 m from the vibration source in the case of the Poisson's ratio ν = 0.25 and train speed V = 300 km/h. As shown in Figure 9, the displacement spectrum of the location in front of the trench is larger than that behind the trench. The amplitude of ground surface vibration behind the open trench was reduced, especially at frequencies higher than 20 Hz. This indicates that an open trench can attenuate the higher-frequency vibration. Ground surface vibration is mainly contributed by shear waves and Rayleigh waves because they carry the most energy during propagation. The shear and Rayleigh wave velocities were close (approximately 250 m/s) and corresponded to a wavelength of less than 12.5 m (at frequencies higher than 20 Hz). Hence, the S wave and the R wave were filtered out by the open trench at a depth of H = 3 m. If the velocity of the S wave and R wave are fixed and the Poisson's ratio ν = 0.45 replaces 0.25, the velocity of the P wave would increase to 900 m/s, resulting in the spectrum figure shown in Figure 10. Figures 9 and 10 show the same trends. This may have occurred because the wavelength of the P wave mainly changed with Poisson's ratio; however, the influence on the spectrum was nonsignificant because the propagating energy of the P wave was limited. The state of the vibration source would change if the speed of the train decreases to 180 km/h. The period of the trainload increased because of the decrease in train speed. As shown in Figure 11, the amplitude on the ground surface in the front of the open trench is larger in frequency (f = 20 Hz). It also shows that the cutoff frequency increased to 30 Hz when the depth of the trench was H = 3 m.

4.3. Screening Effectiveness Evaluated by 1/3 Octave Band Spectrum Analysis. The 1/3 octave band spectrum analysis was used to evaluate the energy of vibration in the frequency domain. Therefore, vibration time history at the location of 2 m behind an open trench was transformed to a 1/3 octave band spectrum to evaluate the screening effectiveness of the open trench. The reducing displacement level (RDL) represents the screening effectiveness using an open trench and can be expressed as follows [11]:

$$\mathrm{RDL} = 20\log_{10}\frac{\sigma_v(\vec{x}, f_c)_{\text{without trench}}}{\sigma_v(\vec{x}, f_c)_{\text{with trench}}}, \tag{11}$$

where the $\sigma_v(\vec{x}, f_c)$ is the particle root mean square displacement vibration value; $\vec{x}$ is the distance of the observing point behind the trench ($\vec{x}$ = 2 m in this study); and f_c is the center

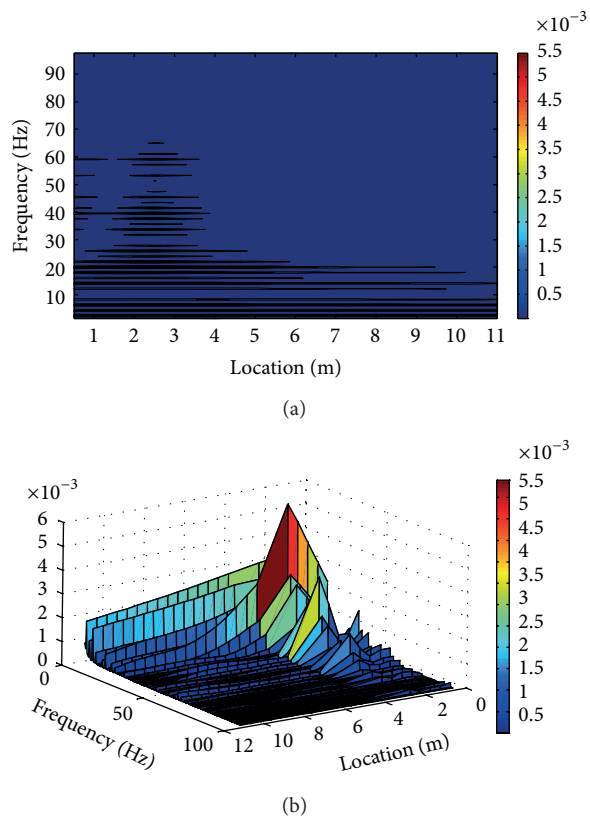

Figure 11: Location-frequency figure with an open trench of L = 10 m, W = 1 m, and H = 3 m (a) contour plot of displacement spectrum on ground surface and (b) surface plot of displacement spectrum on ground surface (Poisson's ratio ν = 0.25, train speed V = 180 km/h). Note: the location coordinate of trench is from 2.5 to 3.5 m.

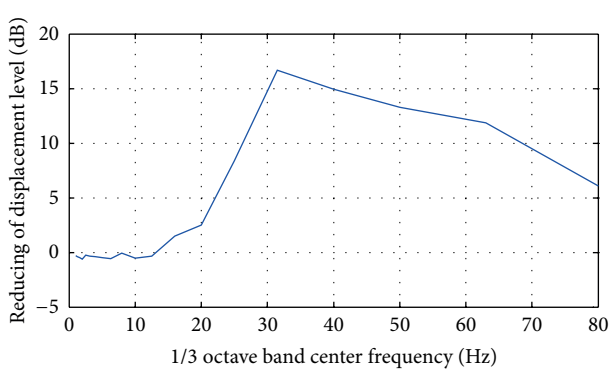

Figure 12: RDL on the location of 2 m behind open trench (L = 10 m, W = 1 m, and H = 3 m; Poisson's ratio ν = 0.25; train speed V = 300 km/h).

frequency in the 1/3 octave band. The RDL is represented as decibel (dB) scale.

A typical case study was performed for an open trench using the following parameters: W = 1 m, L = 10 m, and H = 3 m. The speed of the train was 300 km/h. The RDL from the 1/3 octave band spectrum analysis is shown in Figure 12. The results also indicated that vibrations less than 20 Hz cannot

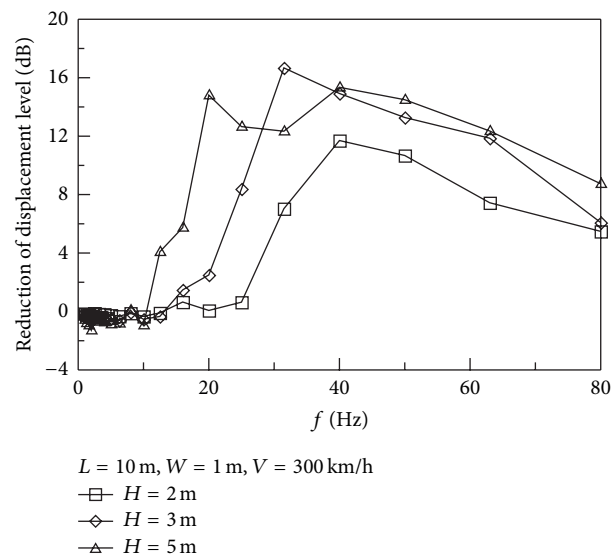

Figure 13: Influence of trench depth on RDL.

be attenuated by a trench using the current configuration. The optimal screening effectiveness occurs at a frequency of 30 Hz.

The effect on vibration reduction of the trench depth H was further examined. All other parameters were maintained at constant values (train speed of V = 300 km/h, Poisson's ratio of ν = 0.25, trench width of W = 1 m, and location of L = 10 m). The optimal screening frequency decreased with increasing trench depth, as shown in Figure 13. Figure 13 shows that the frequency spectrum shifted to the left side with increasing depth of the open trench. The cutoff frequencies of the spectrum for trench depths of H = 2, 3, and 5 m were about 25, 15, and 10 Hz, respectively. The maximal screening frequencies of H = 2, 3, and 5 m were about 40, 30, and 20 Hz, respectively. The Rayleigh wave velocity of soil was assumed as 250 m/s. Figure 11 shows that the maximal screening effectiveness occurred when the depth of the open trench was 0.3-0.4λ_R. The wavelength increases with decreasing the frequency of wave in soil medium. When the wavelengths of the low-frequency waves are higher than trench depth, most of wave energy can be propagated to ground surface behind the trench. Therefore, to reduce the low-frequency vibration, a deeper open trench is necessary.

As shown in Figure 14, the influence of trench width on screening effectiveness is nonsignificant, except for frequencies from 30 to 40 Hz. However, the optimal intercept frequency was approximately 30 Hz in these trench cases. The effect of location of an open trench on RDL is shown in Figure 15. L = 10 m is the optimal location of the trench for a frequency range of 30–50 Hz. However, the RDL is slightly larger in the case of $L \geq 15$ m for a range of 50–80 Hz. In this study, all train speeds were less than the Rayleigh wave velocity of soil. The influence of train speed on RDL is nonsignificant, as shown in Figure 16. To examine the effect of the P wave on reducing vibration using an open trench, three Poisson's ratios of soil were analyzed. Among the three

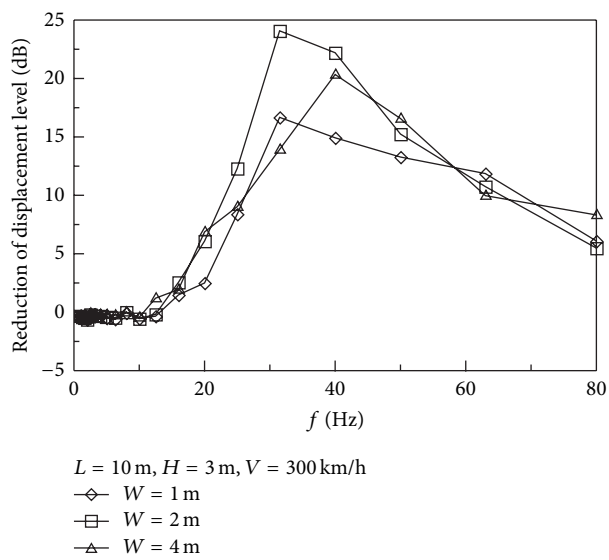

Figure 14: Influence of trench width on RDL.

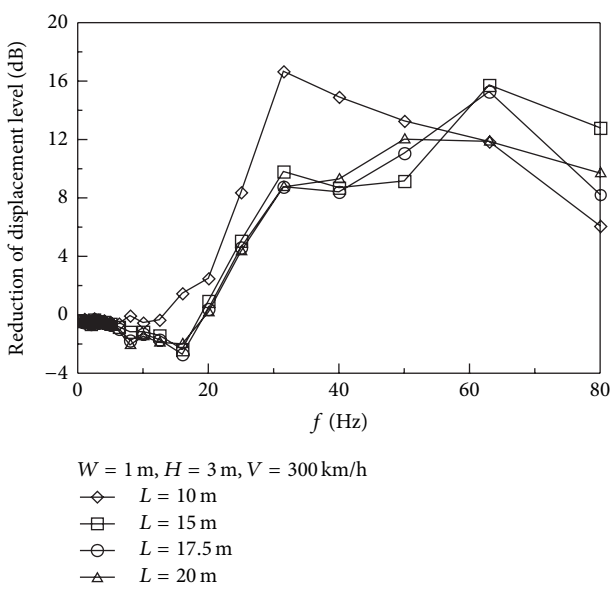

Figure 15: Influence of trench location on RDL.

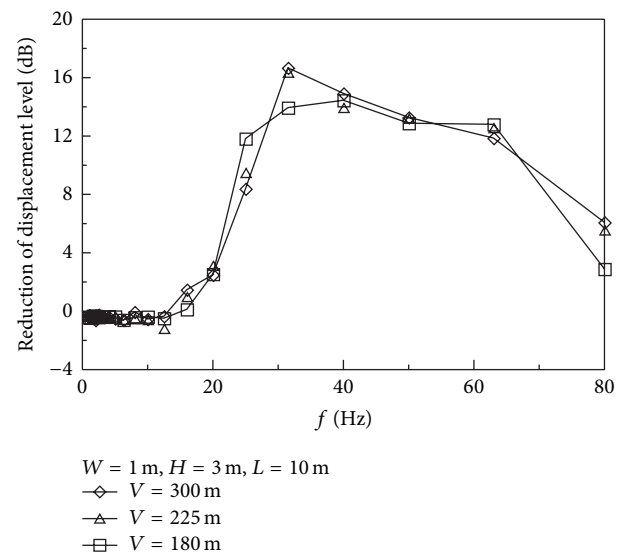

Figure 16: Influence of train speed on RDL.

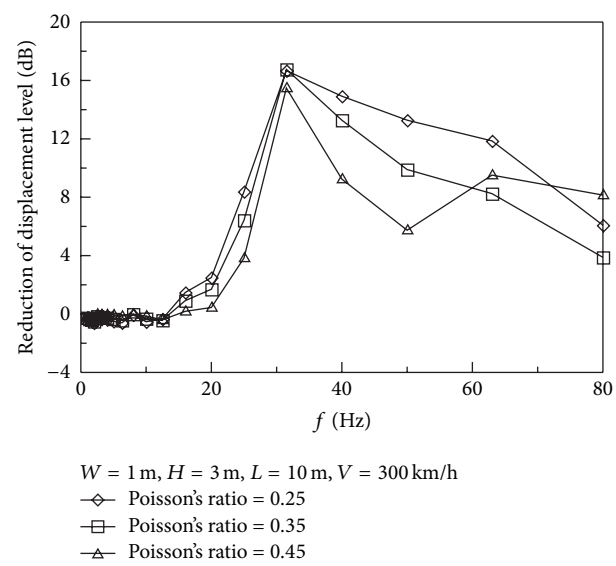

Figure 17: Influence of soil Poisson's ratio on RDL.

cases shown in Figure 17, the optimal intercept frequency was 30 Hz. Poisson's ratio has various effects on the RDL at frequencies higher than 30 Hz. A drop of 8 dB occurs between the Poisson's ratio of 0.25 and 0.45 at 40 Hz. This occurs because Poisson's ratio only affects the P wavelength.

The 1/3 octave band spectrum analysis showed that the maximal reduction of vibration is approximately 25 dB because of the open trench. The RDL is 25 dB, which indicates that the ground displacement amplitude with the existence of an open trench is 1/17.8 times the amplitude without an open trench, as shown in (11). The screening effectiveness of an open trench was considerable from 30 to 70 Hz, as shown in Figures 13–17. The frequency range matches the main frequencies of vibration induced by THSR.

5. Conclusions

Current study applies the 2D time-domain BEM to examine the screening effectiveness of open trenches on reducing vibration generated by HSTs. The dominant frequency range (30–70 Hz) for reducing ground vibration using an open trench matches the main frequencies of vibration induced by HSTs. The main findings are summarized as follows.

(1) The HST-induced vibration is a transient wave propagation problem. A time-domain BEM is thus more appropriate though less commonly used due to its complexity.

(2) The BEM simulations confirm that an open trench can effectively reduce the main frequencies induced by HSTs that has been observed to have a dominant

range of 30–70 Hz in field measurements. The use of location-frequency figures further illustrates the isolation effectiveness of an open trench. Using an open trench as a wave barrier can reduce 10–25 dB of vibration amplitude at frequencies between 30 and 70 Hz.

(3) Additional ABAQUS simulation for the wheel-rail-sleeper model was performed. In wheel-rail-sleeper system, more high-frequency vibrations were generated because of more impulses in the load time history.

(4) The results of the parametric study show that the optimal screening frequency decreases with increasing trench depth. The maximal screening effectiveness occurs when the depth of the open trench is 0.3-0.4λ_R. The influence of trench width on screening effectiveness is nonsignificant, except for frequencies from 30 to 40 Hz. Location of the trench $L = 10$ m is the optimal location of the trench for a frequency range of 30–50 Hz. Poisson's ratio has various effects on the reduction of vibration at frequencies higher than 30 Hz.

Conflict of Interests

The authors declare that there is no conflict of interests regarding the publication of this paper.

Acknowledgments

This work was supported by the National Science Council of Taiwan (NSC98-2221-E-324-026). Their support is gratefully appreciated. The authors are grateful to the National Center for High-Performance Computing for computer time and facilities in this study.

References

[1] G. Degrande and L. Schillemans, "Free field vibrations during the passage of a thalys high-speed train at variable speed," *Journal of Sound and Vibration*, vol. 247, no. 1, pp. 131–144, 2001.

[2] L. Hall, "Simulations and analyses of train-induced ground vibrations in finite element models," *Soil Dynamics and Earthquake Engineering*, vol. 23, no. 5, pp. 403–413, 2003.

[3] P. Galvín and J. Domínguez, "Experimental and numerical analyses of vibrations induced by high-speed trains on the Córdoba-Málaga line," *Soil Dynamics and Earthquake Engineering*, vol. 29, no. 4, pp. 641–657, 2009.

[4] S. H. Ju, H. T. Lin, and J. Y. Huang, "Dominant frequencies of train-induced vibrations," *Journal of Sound and Vibration*, vol. 319, no. 1-2, pp. 247–259, 2009.

[5] K. Emad and G. D. Manolis, "Shallow trenches and propagation of surface waves," *Journal of Engineering Mechanics*, vol. 111, no. 2, pp. 279–282, 1985.

[6] D. E. Beskos, B. Dasgupta, and I. G. Vardoulakis, "Vibration isolation using open or filled trenches, part 1 : 2-D homogeneous soil," *Computational Mechanics*, vol. 1, no. 1, pp. 43–63, 1986.

[7] B. Dasgupta, D. E. Beskos, and I. G. Vardoulakis, "Vibration isolation using open or filled trenches, part 2: 3-D homogeneous soil," *Computational Mechanics*, vol. 6, no. 2, pp. 129–142, 1990.

[8] S. Ahmad and T. M. Al-Hussaini, "Simplified design for vibration screening by open and in-filled trenches," *Journal of Geotechnical Engineering*, vol. 117, no. 1, pp. 67–88, 1991.

[9] P. H. Tsai and T. S. Chang, "Effects of open trench siding on vibration-screening effectiveness using the two-dimensional boundary element method," *Soil Dynamics and Earthquake Engineering*, vol. 29, no. 5, pp. 865–873, 2009.

[10] H. Takemiya, "Field vibration mitigation by honeycomb WIB for pile foundations of a high-speed train viaduct," *Soil Dynamics and Earthquake Engineering*, vol. 24, no. 1, pp. 69–87, 2004.

[11] H. H. Hung, Y. B. Yang, and D. W. Chang, "Wave barriers for reduction of train-induced vibrations in soils," *Journal of Geotechnical and Geoenvironmental Engineering*, vol. 130, no. 12, pp. 1283–1291, 2004.

[12] L. Andersen and S. R. K. Nielsen, "Reduction of ground vibration by means of barriers or soil improvement along a railway track," *Soil Dynamics and Earthquake Engineering*, vol. 25, no. 7–10, pp. 701–716, 2005.

[13] A. Karlström and A. Boström, "Efficiency of trenches along railways for trains moving at sub- or supersonic speeds," *Soil Dynamics and Earthquake Engineering*, vol. 27, no. 7, pp. 625–641, 2007.

[14] Z. Cao, Y. Cai, A. Boström, and J. Zheng, "Semi-analytical analysis of the isolation to moving-load induced ground vibrations by trenches on a poroelastic half-space," *Journal of Sound and Vibration*, vol. 331, no. 4, pp. 947–961, 2012.

[15] D. Younesian and M. Sadri, "Effects of the trench geometry on vibration mitigation level in high-speed railway tracks," *Journal of Mechanical Science and Technology*, vol. 26, no. 8, pp. 2469–2476, 2012.

[16] E. Celebi and O. Kırtel, "Non-linear 2-D FE modeling for prediction of screening performance of thin-walled trench barriers in mitigation of train-induced ground vibrations," *Construction and Building Materials*, vol. 42, pp. 122–131, 2013.

[17] A. S. M. Israil and P. K. Banerjee, "Two-dimensional transient wave-propagation problems by time-domain BEM," *International Journal of Solids and Structures*, vol. 26, no. 8, pp. 851–864, 1990.

[18] M. Adam and O. Von Estorff, "Reduction of train-induced building vibrations by using open and filled trenches," *Computers and Structures*, vol. 83, no. 1, pp. 11–24, 2005.

[19] A. S. M. Israil and P. K. Banerjee, "Advanced time-domain formulation of BEM for two-dimensional transient elastodynamics," *International Journal for Numerical Methods in Engineering*, vol. 29, no. 7, pp. 1421–1440, 1990.

[20] M. Misiti, Y. Misiti, G. Oppenheim, and J. M. Poggi, *Matlab Wavelet Toolbox User's Guide*, The MathWorks, Natick, Mass, USA, 2010.